GeroScience (2024) 46:5303–5320
https://doi.org/10.1007/s11357-024-01128-w

ORIGINAL ARTICLE

Age-related changes in human brain functional connectivity using graph theory and machine learning techniques in resting-state fMRI data

Sepideh Baghernezhad · Mohammad Reza Daliri

Received: 5 November 2023 / Accepted: 8 March 2024 / Published online: 18 March 2024

Abstract Aging is the basis of neurodegeneration and dementia that affects each endemic in the body. Normal aging in the brain is associated with progressive slowdown and disruptions in various abilities such as motor ability, cognitive impairment, decreasing information processing speed, attention, and memory. With the aggravation of global aging, more research focuses on brain changes in the elderly adult. The graph theory, in combination with functional magnetic resonance imaging (fMRI), makes it possible to evaluate the brain network functional connectivity patterns in different conditions with brain modeling. We have evaluated the brain network communication model changes in three different age groups (including 8 to 15 years, 25 to 35 years, and 45 to 75 years) in lifespan pilot data from the human connectome project (HCP). Initially, Pearson correlation-based connectivity networks were calculated and thresholded. Then, network characteristics were compared between the three age groups by calculating the global and local graph measures. In the resting state brain network, we observed decreasing global efficiency and increasing transitivity with age. Also, brain regions, including the amygdala, putamen, hippocampus, precuneus, inferior temporal gyrus, anterior cingulate gyrus, and middle temporal gyrus, were selected as the most affected brain areas with age through statistical tests and machine learning methods. Using feature selection methods, including Fisher score and Kruskal–Wallis, we were able to classify three age groups using SVM, KNN, and decision-tree classifier. The best classification accuracy is in the combination of Fisher score and decision tree classifier obtained, which was 82.2%. Thus, by examining the measures of functional connectivity using graph theory, we will be able to explore normal age-related changes in the human brain, which can be used as a tool to monitor health with age.

Keywords Functional connectivity · Age-related change · Graph theory · Human connectome project · fMRI data · Machine learning techniques

S. Baghernezhad · M. Daliri (✉)
Neuroscience & Neuroengineering Research Lab, Biomedical Engineering Department, School of Electrical Engineering, Iran University of Science and Technology (IUST), Tehran, Iran
e-mail: daliri@iust.ac.ir

Introduction

Aging is the basis of neurodegeneration and dementia that affects every organ in the body. The degeneration associated with normal aging in the brain is associated with progressive slowness and impairment of various abilities, such as motor ability [1]. Performance in various fields of cognitive function also decreased with age [2]. As global aging intensifies, more research is focused on how the brain changes in the elderly. During the natural aging process, the brain changes due to neurological processes such as cell growth, cell death, and atrophy [3]. Adults show a decreased processing speed, attention, working, and episodic memory with age [4].

Often, the incidence of diseases such as Parkinson's and Alzheimer's increases with age and the brain changes caused by aging. Therefore, studying brain changes from youth to old age can help identify the brain areas involved in such disorders.

In recent years, significant research has been devoted to neuroimaging techniques in structural and functional fields to help understand the brain differences of people with different ages. Functional magnetic resonance imaging (fMRI) is a non-invasive method for investigating brain functions that change with different conditions of the experiment or task. fMRI uses blood oxygen level-dependent (BOLD) signal changes to assess brain function and detect changes in brain activity [5].

Many studies on fMRI are performed at a resting state. A resting state is a condition that a person is fully conscious but does not perform any specific cognitive or behavioral activity. In this case, there are more comfortable clinical conditions than when the recording is associated with a specific stimulus or activity. Therefore, studies to track changes in brain activity often use resting state fMRI [6].

Traditionally, three categories of connectivity patterns have been considered for the analysis of fMRI data: Structural connectivity, Functional connectivity, and effective connectivity [7, 8]. Structural connectivity indicates anatomical and physical connections between different brain regions [8, 9]; Functional connectivity consists of methods in which statistical information can be examined between different brain regions and shows the relationships and interactions between these regions, while effective connectivity examines the direct impact of one region on other regions and expresses the causal relationship between regions [8, 10].

Recent age-related brain changes studies have shown that the human brain undergoes significant changes in functional connectome across the lifespan [11–13]. The connectome is defined as a network architecture of functional connectivity between distinct brain structures that act like a "fingerprint" to distinguish individual differences [14–17].

One research field developed in recent years considers the human brain as a complex network consisting of many elements interacting functionally with each other [18]. By modeling this complex network as a graph consisting of nodes (i.e., brain regions or single neurons or voxels) and edges (i.e., conditional dependencies between brain regions or single neurons or voxels for demonstrating structural or functional connectivity), a systematic and topological study of the functional or descriptive organization of brain can be established [19].

In recent years, this method has been widely used in various studies to analyze fMRI data for normal or damaged brains, differences between age groups, and so on [20]. Most new approaches to brain differences between age groups have focused on the whole brain, modeling on predefined ROIs, and studying resting state data [21].

Varangis et al. [21] applied graph theory analysis using resting-state fMRI to investigate and compare changes in the brain networks between the young and old groups. Their study demonstrated increased participation coefficient values in older age resting state networks. They also found that each primary sensory and cognitive brain network was associated with a degree of age-related decline. In another study [22], they found that each primary sensory and cognitive network of the brain was associated with a degree of age-related decline. Also, they examined a variety of functional connectivity measures in four cognitive domains, including vocabulary, processing speed, fluid reasoning, and episodic memory. Their findings show that while aging may generally be associated with reductions in system segregation, within or between-network connectivity, global efficiency, and modularity, the extent and presence of these effects will vary based on the task performed.

Other studies also used electroencephalography to investigate the relationship between age and brain changes. For example, Javaid et al. [22] used graph theory to understand age-related changes in brain function and behavior. Their study showed a significant decrease in network topology features with increasing age and in the elderly group. Features such as global efficiency and clustering coefficient were significantly lower in the elderly group than in the middle-aged group.

In order to help diagnose and be aware of developmental disorders and neuropsychiatric diseases, it is necessary to study changes in different age groups. According to previous studies, to the best of our knowledge, most studies have examined the differences between the young and old age groups or the middle-aged and older age groups, and a few studies have included the under-18 age range. In this study, we have examined 17 cases of graph measures in order to examine brain differences from the perspective of graph theory, from different aspects. As far as we know, there is no such extensive review in previous studies. Also, due to data recording problems in young age groups, studies that examine these groups are limited. Therefore, the various aspects of brain communication related to the age group under 18 years have not been well investigated.

In this study, we evaluate brain differences in the three age groups including 8 to 15 years, 25 to 35 years, and 45 to 75 years, using lifespan pilot data from the Human Connectome Project (HCP). We have also used machine learning techniques based on selecting the most relevant features with age changes through employing a statistical test and Fisher score feature selection and support vector machine (SVM), decision tree (DT), and k nearest neighbors (KNN) classifiers.

The remaining sections of this paper will describe the characteristics of the participants and fMRI data acquisition procedures. Then, the steps for fMRI data analysis, graph metrics calculation, feature selection, and classification will be fully explained. Finally, the obtained results will be reported and discussed.

We organized our study into four sections, including Introduction, Materials and Methods (data details and methodology), Results (our findings), and Discussion (Review of the results and compare with past work).

Materials and methods

The overall procedure is illustrated in Fig. 1. The analysis steps are explained in the following sections.

Subjects

This study includes a total of 40 subjects from the resting state fMRI data of the Human Connectome project (HCP). The dataset consists of two parts: Lifespan pilot fMRI data, including 27 healthy subjects and 13 subjects from 1200 Human Connectome Project subjects identical in acquisition to the lifespan pilot set. Finally, the new category ranges from 8 to 15 years (n = 12; male = 4, female = 8), 25 to 35 years (n = 18; male = 9, female = 9), and 45 to 75 years (n = 10; male = 6, female = 4). This collection of data is available to the public at https://db.humanconnectome.org.

Data acquisition

The Lifespan pilot HCP data was acquired on a 3 Tesla Siemens Connectome MRI scanner at Washington University. The resting state fMRI was acquired with a voxel resolution of $2 \times 2 \times 2$ mm^3, 72 slices, flip angle = 52∘, multi-band factor = 8, and FOV= 810×936 mm^2. Each run was composed of 420 frames using TR= 0.72 s and an echo time (TE) of 33.2 ms. The structural images were acquired using a high-resolution three-dimensional T1-weighted MPRAGE at a resolution of 0.8 mm isotropic voxels.

fMRI pre-processing

fMRI data from Human Connectome Project (HCP) [24] were analyzed using FEAT fMRI analysis option on FSL (FMRIB's Software Library, www.fmrib.ox.ac.uk/fsl) toolbox [14–16]. Images were pre-processed in several steps, including motion correction using MCFLIRT [25] to refine the effects of head movements, spatial smoothing using a Gaussian filter with 5.0 mm^3 full width at half maximum (FWHM), high-pass temporal filtering, non-brain elimination by brain extraction tool (BET), and mapping into the MNI space using FLIRT [18, 19].

Brain anatomical parcellation

The whole brain of each subject was divided into 116 distinct brain structures (regions of interest (ROIs)) with the Automated Anatomical Labeling (AAL) atlas, which includes cortical and subcortical regions from 1 to 90 and also cerebellar areas of 91 to 116 [26]. Each 116 brain region contains a number of voxels, and by averaging the BOLD time series of these voxels, the region's representing time series will be obtained. Fig. 2 shows some examples of several regional time series.

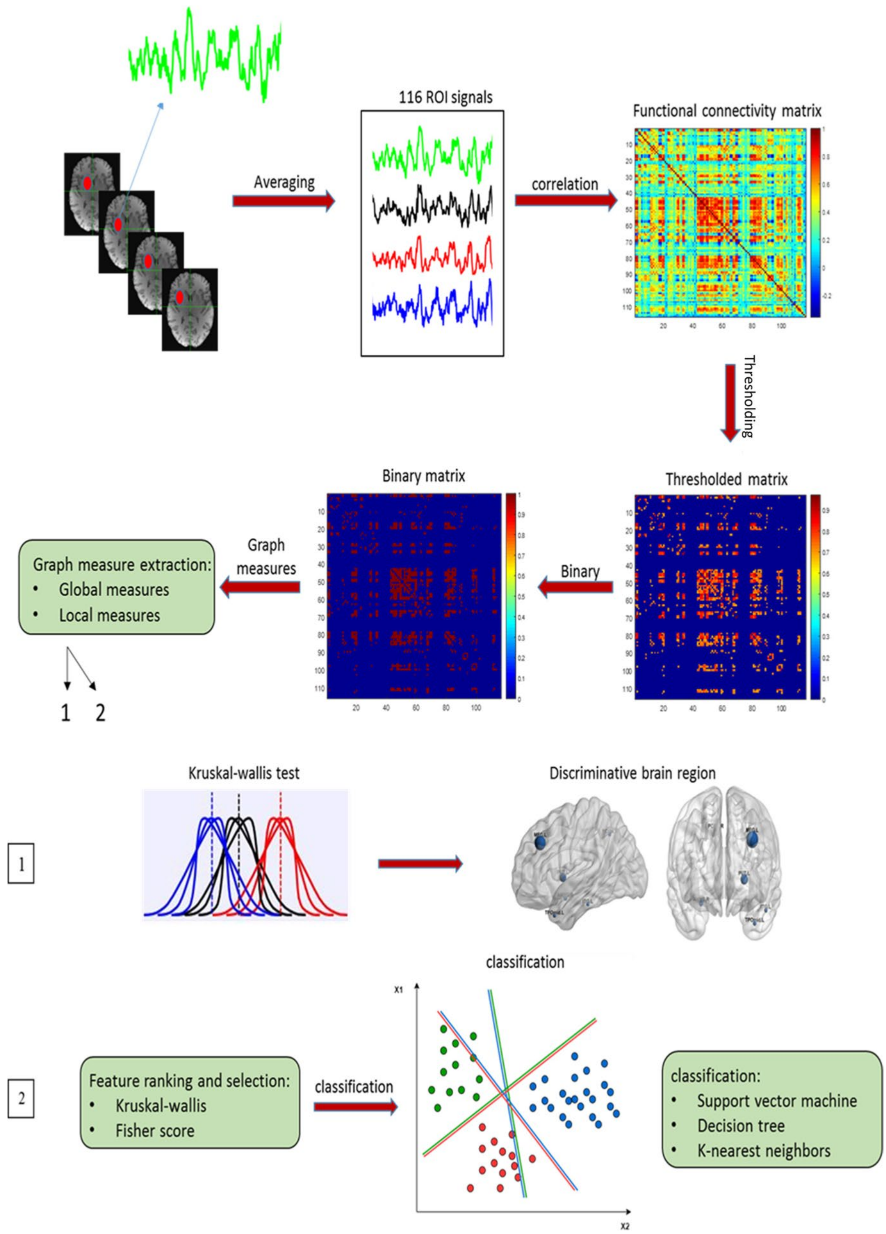

Fig. 1 Scheme of the proposed analyses steps

Pearson correlation coefficients

Pearson correlation was used to calculate the relationship between every two time series of 116 brain regions for the construction of functional connectivity networks. The Pearson correlation coefficient (CC) between two time series (x and y) is [27]:

$$CC = \frac{\sum_k \left(x(k) - \overline{x}\right)\left(y(k) - \overline{y}\right)}{\sqrt{Var(x)Var(y)}} \tag{1}$$

Therefore, the correlation matrix of 116 × 116 of each subject can be obtained. The created functional connectivity matrix is considered a graph, and each of the 116 brain regions is considered nodes of this

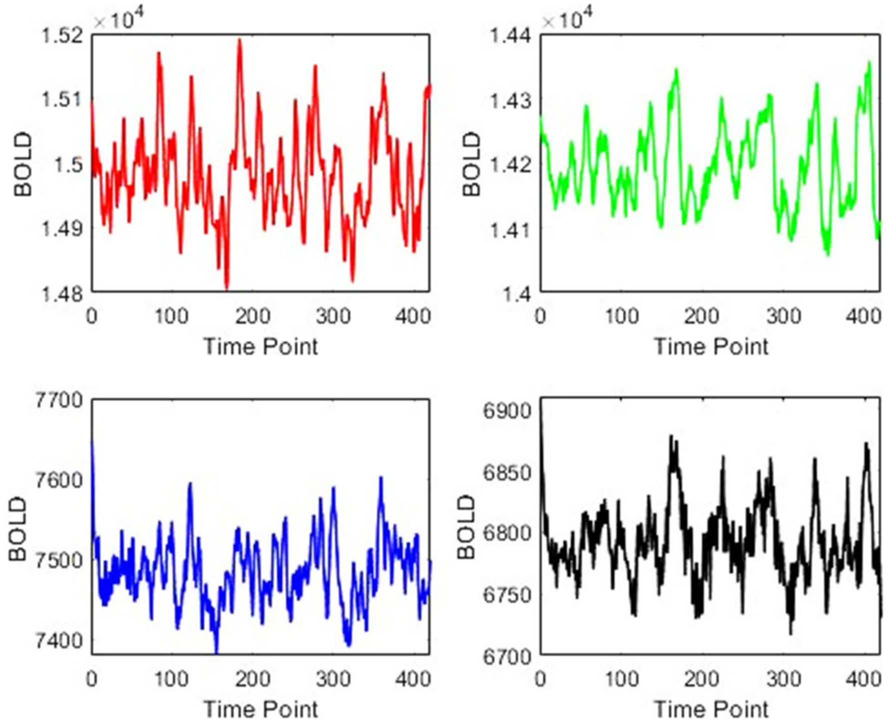

Fig. 2 Time series representation of two brain region for two representative participants. Right Cuneus area of a young subject (CUN.R)(Red Chart), Right Cuneus area of an old subject (CUN.R) (Green Chart), Right Heschl gyrus of a young subject (HES.R)(Blue Chart), and Right Heschl gyrus of a old subject (HES.R)(Black Chart)

graph and the calculated Pearson correlation coefficients are expressed as a measure of connectivity between regions.

Adjacency matrices thresholding

Most graph metrics require sparse graphs [12, 22]. Therefore, in the functional connectivity graph, it is necessary to remove noisy and insignificant information that has low weights and is considered weak connectivity. Hence, functional connectivity matrices were thresholded by preserving a proportion of the strongest connections. In the process of reconstructing the networks of functional connectivity in the brain, this technique is used to ensure equal density between different groups.

In this method, called proportional thresholding, m% of the strongest connections are maintained in the adjacency matrix, and the other connections are removed. In fact, a kind of connection density matching is created that is necessary to compare the characteristics of the network in different groups [28]. Thus, the proportional threshold (TH) values are based on the proportion of preserved links to the total number of links [29]. Proportional thresholding values were employed by preserving 0.02–0.5 of the strongest connections with a step size of 0.01. It should be noted that, after the analysis, we found that the other thresholds do not provide useful information, and this threshold range is considered to reduce the computational cost.

Forty-nine thresholded networks were obtained corresponding to each weighted network due to the selected thresholding range. Finally, each thresholded network was converted to a binary matrix by replacing the elements which were non-zero to 1 and 0 otherwise.

Graph-theoretical measures

Graph measures were evaluated according to several perspectives, including functional segregation, functional integration, and centrality [29–31]. Functional segregation examines the brain's ability to perform specialized processes within densely interconnected areas. Functional integration examines the brain's efficiency in combining information from different domains. Centrality measures can assess the importance of a node in terms of interaction with other nodes.

In this study, in terms of functional segregation, global graph measures including modularity [32, 33], mean clustering coefficient [33, 34], mean local efficiency [35], and transitivity [34] were examined. As a measure of functional integration, global efficiency and characteristic path length [36, 37] were evaluated. Small world networks [38, 39] and assortativity measures were also calculated as other global measures.

For local measures, degree [40], betweenness centrality [33], K-coreness centrality [41], sub-graph centrality, Eigenvector centrality [42], local efficiency, participation coefficient [43], diversity, and node strength were calculated. These features were calculated using the BCT and GraphVar toolbox [37, 44].

Thus, 49 functional connectivity measures were obtained for each subject, and for each of these measures, one global value and 116 (number of ROIs) local values were obtained.

Statistical tests

After extracting the brain network measures, the Kruskal-Wallis test [45, 46] with correction by using false discovery rate (FDR) was employed to determine the significant differences between the three groups in global and local measures. The Kruskal-Wallis test is a popular nonparametric method that assesses the differences among three or more independently sampled groups when the distribution of the data is not normal. To draw conclusions about the differences among the three groups, a post hoc Mann-Whitney *U* test was performed using the Holm-Bonferroni method, which aligns with the Kruskal-Wallis testing approach.

The discriminative graph measures identified based on the corresponding resulted *p* values with a significance level of 0.05 (with FDR-correction). We considered a region to be discriminative between the three groups (8–15 years, 25–35 years, 45–75 years) if the brain regions were significantly different over more than half of the binary graphs (more than 24).

Feature ranking and classification

We ranked the features using two methods. The first method was using Kruskal-Wallis statistical test, which the features were sorted in ascending order based on *p* value, and in the feature selection process, features with the lowest *p* value were selected.

In the second method, we used the Fisher score [47–49] to identify the best measures among all features. We tested several feature ranking methods, including RelifF [50], mRMR [51], and Fisher score. Finally, we chose the Fisher score because it leads to the best results in classification accuracy. Fisher score shows the distinction power of each feature by determining a score for each feature. Fisher score can be derived from the following statement:

$$fisher - score = \frac{\sum_{i=1}^{c} n_i(m_i - m)^2}{\sum_{i=1}^{c} n_i \sigma_i^{\,2}} \quad (2)$$

That m and σ are the mean and standard deviation in the whole data set, and *mi* and σ*i* are the mean and the standard deviation of the features in each class. Also, C is the number of classes, i is the label of each class, and n_i is the number of subjects in class i. The larger Fisher score shows a greater ability to distinguish between classes.

In this study, three classifications including support vector machine (SVM) with linear kernel function with various parameters [52, 53], decision tree (DT) [54], and k nearest neighbors (KNN) [55] have been used to classify the three mentioned age groups. SVM is generally proposed for the classification of two classes, but we have generalized it to the three-class mode with a one vs. one approach.

The K-fold method [56] with $k = 10$ has been used as a cross-validation method in the three-class mode to evaluate the performance of classification. In this method, in each run, the feature set is divided into ten parts, and one of the ten parts is used as test data, and the remaining nine parts are used as training data. Finally, the most repetitive features common to the ten steps of cross-validation in the training step were introduced as distinctive features.

Result

In this research, Kruskal-Wallis test and Fisher score were employed on graph measures obtained from binary adjacency matrices to distinguish three age groups. The analysis results are described in the following sections.

Statistical analysis of global graph characteristics

To examine the significant differences in the global measures, in 2 to 50% of the strongest connection, we have analyzed the values of the graph characteristics obtained from three different groups by Kruskal-Wallis test and report as follows:

Global efficiency: The ability to integrate information into brain areas can be assessed by global efficiency [57]. High-level functions, such as executive functions that require integrating information from different sources, benefit from global network efficiency [58]. The global efficiency was significantly different in 19–28% of preserved strongest weights, and the lowest p value is at TH= 25% and equal to 0.0181. Other thresholds that are statistically significant are shown in Fig. 3a. We observe a decrease in global efficiency with age. Between the ages of 8 and 15, shown in the red chart, the highest global efficiency is observed, followed by a decrease in young people, and finally, the lowest in the middle-aged and older groups. Some studies have confirmed a decline in global efficiency with age [58, 59]. Most studies have examined the changes in brain networks in a specific age range (for example, middle-aged and old [59]), but, a wider age range has been considered in this study.

Transitivity: Transitivity as a network segregation metric was statistically significant in most thresholds. We observed significantly different over a wide range of proportional thresholding from TH = 0.12 to 0.27 (the lowest p value is at TH= 0.15 and equal to 0.0309). As shown in Fig. 3b, we see an increase in transitivity with age. In the ages of 8 to 15 years, which is shown by the red chart, the lowest amount of transitivity is observed, and then this amount increases slightly in young people in the age group of 25 to 35, and finally, the highest amount belongs to the middle-aged and old group. The higher value of transitivity represents greater specialization of the brain. Some studies confirm our findings about the increasing trend of transitivity with age [59].

Small-worldness: We had significant differences in the small-worldness over the binary graphs in some thresholds (p = 0.0534 at TH = 0.29, p = 0.0299 at TH = 0.3, p = 0.034 at TH = 0.32, p = 0.0406 at TH = 0.33, p = 0.0374 at TH = 0.35, p = 0.0275 at TH = 0.36, p = 0.0240 at TH = 0.37). The small-worldness can be a measure of increased information transfer speed and processing efficiency [40]. Therefore, the differences in the properties of the small world during different age periods can be justified. In many of the mentioned thresholds, the values of the mentioned features were lower in the elderly group, which can be

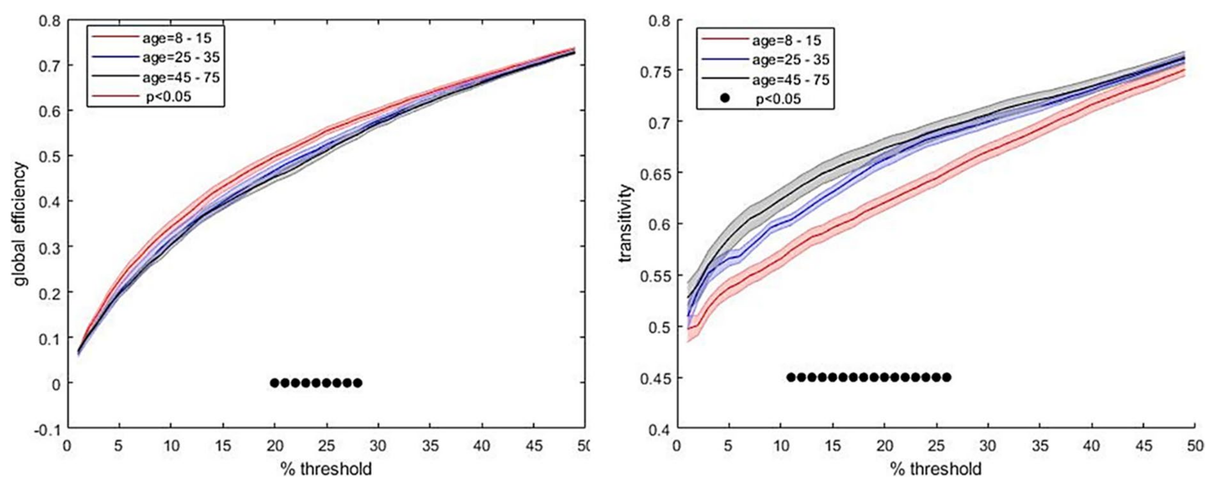

Fig. 3 Changes in global efficiency and transitivity with age changes. The red chart is for the child and adolescent age group, the blue chart is for the young age group, and the black chart is for the middle-aged and older age group. **a** Investigation of changes in global efficiency in three different age groups in at TH = 2 to 50%. The highest value of the global efficiency was observed in children and adolescents. **b** Investigation of changes in transitivity in three different age groups in at TH = 2 to 50%. The highest value of the transitivity was observed in middle-aged and older age group

justified by the decrease in the efficiency and speed of processing in old age.

Other global measures: The other global measures obtained did not differ significantly in any of the proportional thresholds. For example, modular structure, which is one of the measures of functional segregation, is obtained using the Louvian algorithm [60], a fast algorithm for module detection in weighted or binary functional networks. This algorithm has a random phase (greedy optimization), so to select the best case, this algorithm was applied 100 times for each binary network and the structure equivalent to the maximum modularity value was reported. But no significant difference was observed between the groups. Modularity (lowest p value was $p > 0.0619$ at TH = 0.12), assortativity ($p > 0.098$ at TH = 0.07), characteristic path length ($p > 0.081$ at TH = 0.12), and clustering coefficient ($p > 0.093$ at TH = 0.13) were obtained from the analysis.

Statistical analysis of local graph characteristics

Brain areas often interact with many other areas, which plays a key role in network resilience to age changes or disease. Several centrality measures were calculated as local features in each brain area to identify these important areas.

The results of statistical analyses of local measures are shown in Table 1. It should be noted that these results show brain regions that have been able to be localized on over more than half of the thresholded matrices (i.e., thresholded matrices from 2 to 50% of strongest connections) make a significant difference in groups. Post hoc Mann-Whitney U tests (corresponding to the Kruskal-Wallis test) were applied to identify significant differences between pairs of groups. The comparison between some local measures, between three different groups, is shown in the Fig. 4.

We identified the brain regions which could differentiate between three groups in many local graph measures, including right middle frontal gyrus (MFG.L), right amygdala (AMYG.R), paracentral lobule (PCL.L), putamen (PUT.R), temporal pole: middle temporal gyrus (TPOmid.R), and the inferior temporal gyrus (ITG.R). All of the significant regions between the three groups in all network measures are shown in Fig. 5.

Classification

The purpose of the present study was to investigate brain regions and graph measures that were different in resting state fMRI data in the three age groups using AAL atlas. Also, this study aimed to distinguish different age groups to assess the strength of relevant network measures in separating groups using machine learning techniques.

For local features, by employing tenfold cross-validation, we divide the data set into ten parts each time, with one part for testing data and the other for training data, so that the testing folds encompass all three age groups. We used two feature selection techniques: Kruskal-Wallis statistical test and Fisher score. Different sets of top features (up to ten features to avoid over-fitting) were selected for training and testing of the KNN, DT, and SVM classifiers.

The best result of the classification for local measures is reported in Table 2, which was achieved by the different number of ranked features. The highest accuracy was obtained by the combination of Fisher score and decision tree classifier and was equal to 82.2%. This accuracy was obtained using the properties including Local efficiency, K-coreness centrality, Strength, Degree, and Eigen-vector centrality measured in the regions of the anterior cingulate gyrus, left median cingulate gyrus, right putamen, and right precuneus. These measures in their corresponding regions are expressed as discriminative features and informative brain regions that are associated with age-related changes. The Confusion Matrices for the feature selection method/classification method pairs that show highest performance are shown in Fig. 6.

The classification performance for any local graph measure was also computed, and the best achieved classification performances are reported in Table 3. These calculations were done to investigate the discriminatory power of every individual local graph measure between the three mentioned age groups. Also, brain areas that had the most repetition in the feature selection process were reported.

According to Table 3, areas including right putamen, amygdala, hippocampus, percuneus, anterior cingulate gyrus, right inferior temporal gyrus, cerebral cortex, temporal pole: middle temporal gyrus, right middle temporal gyrus, and left inferior parietal have been repeated many times in feature selection process.

Table 1 Significant regions between three age groups in the range of 0.02–0.49 of TH values

ROI	degree	Betweenness centrality	K-coreness centrality	Subgraph centrality	Eigenvector centrality	Local efficiency	Participation coefficient	Diversity	Strength
2						$p=0.0098$ (0.49)			
7	$p=0.017$ (0.38)							$p=0.002$ (0.19)	$p=0.017$ (0.38)
8	$p=003$ (0.24)						$p=0.009$ (0.39)	$p=5.3e^{-4}$ (0.15)	$p=003$ (0.24)
20	$p=0.0117$ (0.21)		$p=0.008$ (0.06)				$p=0.008$ (0.35)	$p=0.0020$ (0.26)	$p=0.0117$ (0.21)
34	$p=0.0134$ (0.38)						$p=0.0051$ (0.18)		$p=0.0134$ (0.38)
38	$p=0.004$ (0.44)		$p=0.0018$ (0.38)		$p=0.0065$ (0.38)				$p=0.004$ (0.44)
40						$p=0.0012$ (0.23)			
42	$p=0.0010$ (0.5)		$p=0.0012$ (0.45)		$p=0.019$ (0.5)		$p=0.0046$ (0.42)	$p=0.0085$ (0.40)	$p=0.0010$ (0.5)
43			$p=0.0045$ (0.3)						
44			$p=0.0012$ (0.24)						
45			$p=0.0119$ (0.1)						
46			$p=0.0010$ (0.07)						
50	$p=6.0e^{-4}$ (0.07)		$p=8.6e^{-5}$ (0.07)		$p=1.4e^{-4}$ (0.08)				$p \approx 0$ (0.07)
52			$p=0.0023$ (0.24)						
57		$p=0.0014$ (0.1)				$p=0.0019$ (0.49)			
61	$p=8.1e^{-4}$ (0.28)	$p=9.5e^{-4}$ (0.14)		$p=0.015$ (0.21)	$p=0.0174$ (0.26)				$p \approx 0$ (0.28)
62	$p=7.1e^{-4}$ (0.36)				$p=0.001$ (0.36)				$p \approx 0$ (0.36)
67	$p=0.005$ (0.16)		$p=7.5e^{-4}$ (0.05)						$p=0.005$ (0.16)
69	$p=0.0104$ (0.14)	$p=0.0012$ (0.33)	$p=0.0049$ (0.07)	$p=0.018$ (0.24)					$p=0.0104$ (0.14)
71	$p=0.0054$ (0.41)	$p=0.001$ (0.39)	$p=0.028$ (0.22)						$p=0.0054$ (0.41)
73	$p=0.0027$ (0.39)	$p=1.2e^{-4}$ (0.31)	$p=0.0031$ (0.36)		$p=0.008$ (0.11)				$p=0.0027$ (0.39)
74	$p=3.4e^{-4}$ (0.21)	$p=4.03e^{-5}$ (0.18)	$p=3.0e^{-4}$ (0.23)		$p=0.002$ (0.12)	$p=0.0067$ (0.38)	$p=1.3\ e^{-4}$ (0.21)	$p=7.8e^{-5}$ (0.21)	$p \approx 0$ (many TH)
76	$p=0.0133$ (0.37)								$p=0.0133$ (0.37)
77					$p=0.0075$ (0.14)				
86						$p=0.004$ (0.27)	$p=1.04\ e^{-4}$ (0.3)	$p=3.9e^{-4}$ (0.19)	

Table 1 (continued)

ROI	degree	Betweenness centrality	K-coreness centrality	Subgraph centrality	Eigenvector centrality	Local efficiency	Participation coefficient	Diversity	Strength
88			$p=0.002$ (0.06)	$p=2.9e^{-4}$ (0.08)	$p=0.001$ (0.07)				
90						$p=2.4e^{-4}$ (0.21)	$p=0.0022$ (0.35)	$p=0.0033$ (0.27)	
92	$p=0.0120$ (0.1)				$p=0.0013$ (0.2)				$p=0.0120$ (0.1)
98						$p=0.0034$ (0.35)			
100					$p=0.012$ (0.34)				

These regions **were significantly different between the three groups** in more than half of the thresholds. The minimum p value and corresponding threshold for each ROI (FDR-corrected, $p<0.05$)

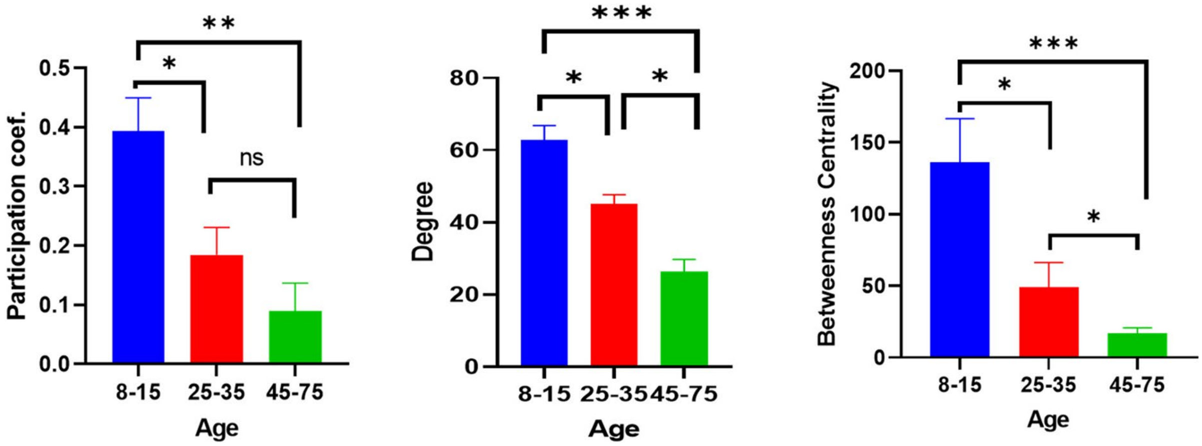

Fig. 4 Comparison of the local measures between three age groups. Data are mean ± SEM. Significant p values from Kruskal–Wallis with Bonferroni post hoc test are indicated (*$p<0.05$, **$p<0.01$, ***$p<0.001$)

Fig. 5 Significant regions in all graph measures between the three groups

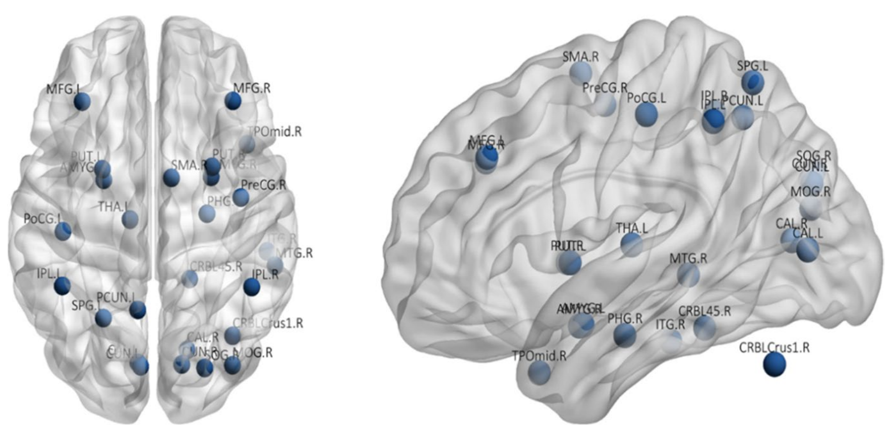

Table 2 Classification performance of the optimal set of ordered features using the fisher score and Kruskal–Wallis test for all local measures

	Classifier	TH	ACC(%)	ROI
Fisher score	SVM	0.21	77.03%	Local efficiency (ACG.L, ACG.R) K-coreness (DCG.L, PCUN.R) Strength (ACG.R) Eigenvector centrality (Degree (ACG.R)
	KNN	0.18	70.55%	Participation coefficient (PUT.R, MTG.R, ITG.R) Degree (PUT.R) Strength (PUT.R)
	DT	0.08	82.22%	Local efficiency (ACG.L, ACG.R) K-coreness (DCG.L, PCUN.R) Strength (PUT.R) Degree (ACG.R) Eigenvector centrality (ACG.R)
Kruskal–Wallis	SVM	0.23	76.66%	Local efficiency (PHG.R, ITG.R) Participation coefficient (PUT.R) Diversity (DCG.L, PUT.R, TPOsup.L, MTG.R)
	KNN	0.21	80%	Local efficiency (PHG.R, ITG.R) Participation coefficient (PUT.R) Diversity (DCG.L, PUT.R, TPOsup.L, MTG.R)
	DT	0.07	67/77%	Local efficiency (ACG.L) K-coreness (DCG.L, PCUN.R) Strength (ACG.R, PUT.R) Eigenvector centrality (ACG.R)

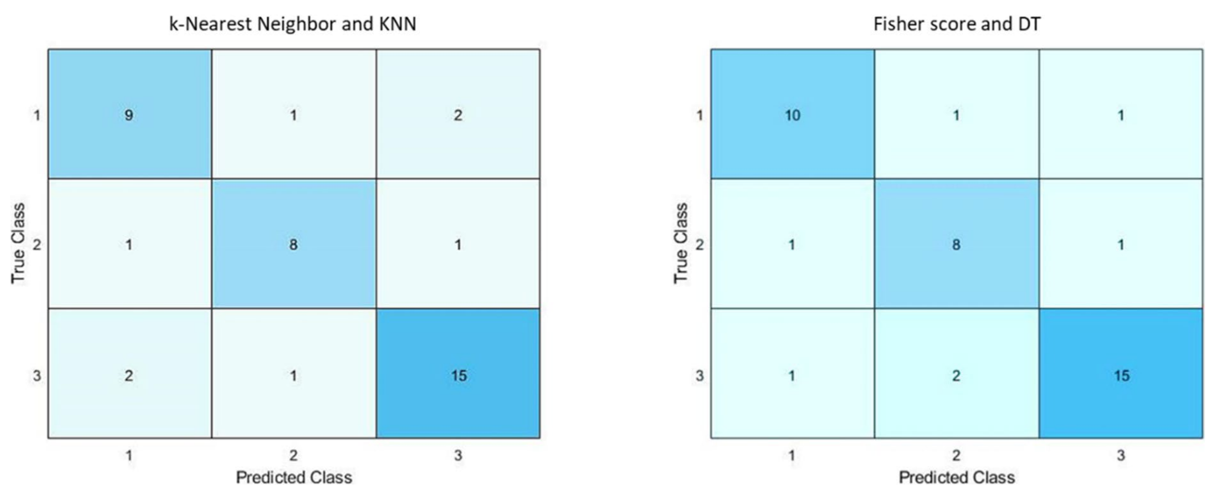

Fig. 6 Confusion matrices for the feature selection /classification method pairs that show highest performance

It can be seen from Table 3 that the best accuracy of 80% was achieved by the individual local measures, including k-coreness centrality and local efficiency, using both the feature extraction method and the decision tree classifier. These results demonstrate the high power of a single k-coreness centrality and local efficiency features in differentiating different age groups.

For global measures, as shown in Table 4, the performance of 62.5% was achieved through two features of global efficiency and transitivity among all global features. This performance was achieved

Table 3 The results of the classification calculated using each of the local measures with Fisher score and Kruskal–Wallis test. The brain areas were parcellated by AAL atlas and labeled with numbers 1 to 116

Feature selection method	Graph measures	DT	KNN	SVM
Fisher score	Degree	ACC = 62.5% TH = 0.38 ROI = 42, 45, 61, 62, 73, 74, 86, 92	ACC = 65.37% TH = 0.1 ROI = 7, 32, 38, 73, 88, 92, 100	ACC = 68.14% TH = 0.06 ROI = 6, 26, 32, 38, 88, 100
	Betweenness centrality	ACC = 65.3% TH = 0.21 ROI = 14, 57, 74, 90	ACC = 70.92% TH = 0.48 ROI = 41, 73, 74, 97, 98	ACC = 70.92% TH = 0.18 ROI = 60, 61, 73, 74, 92
	k-coreness centrality	ACC = **80%** **TH = 0.36** ROI = **42, 43, 45, 61, 73, 74, 92**	ACC = 71.4% TH = 0.03 ROI = 31, 32, 38, 67, 69	ACC = 74.81% TH = 0.31 ROI = 42, 43, 45, 74, 86, 92, 100
	Subgraph centrality	ACC = 64.4% TH = 0.08 ROI = 42, 43, 73, 88, 92	ACC = 64.4% TH = 0.36 ROI = 2, 26, 61, 62, 66	ACC = 62.5% TH = 0.03 ROI = 41, 43, 44, 67, 75, 84, 100
	Eigenvector centrality	ACC = 60.73% TH = 0.18 ROI = 38, 50, 51, 74, 88, 92	ACC = 62.5% TH = 0.03 ROI = 32, 38, 50, 98	ACC = 62.5% TH = 0.04 ROI = 32, 38, 46, 50, 67, 98
	Local efficiency	**ACC = 80%** **TH = 0.21** **ROI = 8, 56, 60, 73, 74, 92**	ACC = 74.81% TH = 0.04 ROI = 26, 31, 32, 50, 60, 68	ACC = 80% TH = 0.04 ROI = 26, 31, 32, 50, 60, 68
	Participation coefficient	ACC = 68.14% TH = 0.4 ROI = 2, 42, 73, 74, 86, 90	ACC = 74.25% TH = 0.39 ROI = 14, 73, 74, 76, 84, 86, 90	ACC = 71.4% TH = 0.41 ROI = 42, 74, 84, 86, 90
	Diversity	ACC = 70.92% TH = 0.21 ROI = 8, 11, 32, 33, 86, 89	ACC = 64.4% TH = 0.25 ROI = 11, 74, 86, 89, 90	ACC = 72.4% TH = 0.18 ROI = 11, 33, 85, 86, 89
	Strength	ACC = 62.5% TH = 0.38 ROI = 42, 45, 61, 62, 73, 74, 86, 92	ACC = 65.37% TH = 10 ROI = 7, 32, 38, 73, 88, 92, 100	ACC = 68.14% TH = 0.06 ROI = 6, 26, 32, 38, 88, 100

in combination of Fisher score and decision tree classifier in TH = 0.18.

Discussion

This study aimed to investigate the changes in the topological characteristics of functional networks obtained from resting state fMRI data in three different age groups: 8 to 15 years, 25 to 35 years, and 45 to 75 years. By applying a 116-regional atlas and then calculating the Pearson correlation between pairs of regions, brain networks were constructed and examined which graph features could distinguish between the three groups.

Amongst the global measures, global efficiency showed a significant difference between age groups in most of the applied thresholds, and we demonstrate a decreasing trend with age. Older adults and middle-aged adults had the lowest global efficiency levels, and these values were higher in young people and children and adolescents. Global efficiency is a tool for assessing functional integrity and information transfer at the global level of the brain [61].

Table 3 (continued)

Feature selection method	Graph measures	DT	KNN	SVM
Kruskal–Wallis	Degree	ACC = 65.37% TH = 0.38 ROI = 42, 45, 50, 61, 62, 73, 74, 92	ACC = 66.29% TH = 0.09 ROI = 6, 32, 50, 74, 88, 100	ACC = 67.77% TH = 0.09 ROI = 6, 32, 50, 88, 92, 100
	Betweenness centrality	ACC = 70.92 TH = 0.14 ROI = 8, 57, 61, 73, 74	ACC = 76.11% TH = 0.31 ROI = 30, 61, 73, 74, 98	ACC = 71.4% TH = 0.16 ROI = 8, 61, 73, 74
	k-coreness centrality	**ACC = 80%** **TH = 0.36** **ROI = 45, 67, 74, 88**	ACC = 69.6% TH = 0.05 ROI = 31, 32, 38, 60, 67	ACC = 74.25% TH = 0.03 ROI = 31, 32, 67
	Sub graph centrality	ACC = 60.73% TH = 0.03 ROI = 31, 32, 50, 61, 69	ACC = 64.4% TH = 0.08 ROI = 43, 50, 69, 88, 90, 98	ACC = 54.62% TH = 0.20 ROI = 43, 61, 69
	Eigenvector centrality	ACC = 69.6% TH = 0.10 ROI = 38, 50, 62, 74, 88, 92	ACC = 69.6% TH = 0.03 ROI = 6, 31, 32, 50, 62, 75	ACC = 64.4% TH = 0.06 ROI = 6, 50, 88
	Local efficiency	**ACC = 80%** **TH = 0.23** **ROI = 8, 74, 90**	ACC = 75.18% TH = 0.04 ROI = 26, 31, 32, 60, 67	ACC = 77.59% TH = 0.23 ROI = 8, 74, 90
	Participation coefficient	ACC = 69.6% TH = 0.03 ROI = 8, 41, 42, 74, 84, 88, 90	ACC = 69.6% TH = 0.31 ROI = 8, 74, 86, 90	ACC = 75.18% TH = 0.19 ROI = 74, 86, 90
	Diversity	ACC = 70.92% TH = 0.22 ROI = 33, 74, 85, 86	ACC = 68.14% TH = 0.21 ROI = 8, 33, 74, 76, 86	ACC = 71.4% TH = 0.21 ROI = 74, 85, 86, 89
	Strength	ACC = 65.37% TH = 0.38 ROI = 42, 45, 50, 61, 62, 73, 74, 92	ACC = 66.29% TH = 0.09 ROI = 6, 32, 50, 74, 88, 100	ACC = 67.77% TH = 0.09 ROI = 6, 32, 50, 88, 92, 100

ROI: 6—Frontal_Sup_Orb_R, ROI: 8—Frontal_Mid_R, ROI: 11—Frontal_Inf_Oper_L, ROI: 26—Frontal_Mid_Orb_R, ROI: 30—Insula_R, ROI: 31—Cingulum_Ant_L, ROI: 32—Cingulum_Ant_R, ROI: 33—Cingulum_Mid_L, ROI: 38—Hippocampus_R, ROI: 41—Amygdala_L, ROI: 42—Amygdala_R, ROI: 43—Calcarine_L, ROI: 45—Cuneus_L, ROI: 50—Occipital_Sup_R, ROI: 56—Fusiform_R, ROI: 60—Parietal_Sup_R, ROI: 61—Parietal_Inf_L, ROI: 67—Precuneus_L, ROI: 73—Putamen_L, ROI: 74—Putamen_R, ROI: 84—Temporal_Pole_Sup_R, ROI: 85—Temporal_Mid_L, ROI: 86—Temporal_Mid_R, ROI: 88—Temporal_Pole_Mid_R, ROI: 89—Temporal_Inf_L, ROI: 90—Temporal_Inf_R, ROI: 92—cereblm_crusl_R, ROI: 100—cerebellum_6_R

Networks can increase their efficiency by randomization. By randomizing the network, an increase in randomized information can reduce the path length and thus increase the global efficiency of the network. Our results are consistent with previous studies showing a reduction in global efficiency [61, 62].

In contrast, transitivity increased with age. Transitivity is a measure of network segregation, which is characteristic of specialized processing and quantifies the presence of interconnected groups in a brain network model [63, 64]. Children and adolescents showed the lowest levels of transitivity, and these values showed an increasing trend in the youth, middle-aged, and old groups, respectively.

Table 4 Classification performances of the optimal sets of global features

	DT	KNN	SVM
Fisher score	ACC = 62.5% TH = 0.18 (global efficiency, transitivity)	ACC = 60.73% TH = 0.38 (global efficiency, transitivity, small_world-ness)	ACC = 54.62% TH = 0.2 (global efficiency, transitivity, mean local efficiency)
Kruskal–Wallis	ACC = 58.33% TH = 0.18 (transitivity)	ACC = 57.4% TH = 0.21 (global efficiency, transitivity)	ACC = 58.33% TH = 0.7 (global efficiency, transitivity, small_world-ness)

The best features in the feature selection process along with the obtained accuracy and the selected threshold are displayed in the table.

Small world property was observed in the brain networks of all age groups. Small world phenomenon indicates an increase in the speed of information transfer and processing efficiency [40]. These values showed significant differences between the three groups in several TH.

Regarding the extracted local measures, significant differences were observed between the groups on most centrality measures, including k-coreness centrality, subgraph centrality, and degree. High degree areas are functionally related to many other areas of the brain [11]. In fact, a higher degree indicates areas that are connected to more areas [33].

The k-coreness centrality identifies sub-graph with high centrality that are denser with a greater number of distinct paths between connected regions. This helps to provide a platform for choosing more appropriate path for information transfer [65]. The subgraph centrality also indicates the nodes participation degree in all network subgraphs.

Region of left middle frontal gyrus (MFG.L), right amygdala (AMYG.R), left paracentral lobule (PCL.L), right putamen (PUT.R), temporal pole: middle temporal gyrus (TPOmid.R), and inferior temporal gyrus (ITG.R) from AAL atlas are brain regions that have shown significant differences between groups in most graph measures.

The medial frontal gyrus is an area associated with high-level executive functions and decision-making processes [66]. Studies have shown age-related decreases in the activation of the prefrontal regions including medial frontal gyrus. The amygdala plays an important role in learning, decision making, and processing of memory and emotional regulation [67]. In previous studies comparing young adults and older adults, it was shown that at older ages, greater functional connectivity between the right amygdala and ventral anterior cingulate cortex was observed, probably reflecting increased emotional regulation [68].

The paracentral lobe controls the motor and sensory nerves of the lower limb and is also responsible for control of defecation and urination. Our findings were compatible with prior reports showing that the topological properties of a number of regions, such as the paracentral lobe, changed significantly from young adulthood to late adulthood [69].

The main function of the right putamen is in motor skills and types of learning. Putamen has been reported frequently in many neurodegenerative diseases. This area plays an important role in perception and is part of the motor apparatus that begins to function to act and do something. Significant differences in the graph measures, including local efficiency and betweenness centrality of putamen between healthy controls (HC), mild cognitive impairment (MCI), and Alzheimer's disease groups (AD), have been shown in Khazaee et al. study [70].

The temporal pole in the right middle temporal gyrus is responsible for face perception. The inferior temporal gyrus is also responsible for processing auditory information, understanding language, and organization. Memory function, motor abilities, cognition, and learning decrease with age. The areas identified by the study emphasize this decreasing trend with age. Our results are consistent with previous studies on changes in these areas.

In addition, this study aimed to distinguish between age groups to assess the strength of relevant graph measures in separating the three groups using machine learning approaches. The best classification performance was obtained using feature selection with Fisher score and DT classifier. This accuracy was equal to 82.22%. The reported accuracy is a cross-validation accuracy on a single dataset, and it is suggested to evaluate the analyses on larger datasets that are not used in any way during the classifier optimization process. Frequent areas in the decision-making process were anterior cingulate gyrus (ROI: 31,32), median cingulate gyrus (POI: 33), parahippocampal gyrus (ROI: 40), right precuneus (ROI: 68), right putamen (ROI: 74), temporal pole: superior temporal gyrus (ROI: 83), middle temporal gyrus (ROI: 86), and inferior temporal gyrus (ROI: 90). These areas were reported to be significantly different in various network measures several times.

Parahippocampal gyrus plays an important role in encrypting and retrieving memory. This area is part of the cortex gray matter that surrounds the hippocampus and is part of the limbic system. The right middle temporal lobe is also involved in reading comprehension. According to the findings of previous studies, these areas also change with age [71]. Aging is associated with cognitive impairment and brain functions such as those involved in attention, memory, motor control, and emotional control [72].

The classification performance for any individual local measure was also computed to investigate the discriminatory power of single local measures between three age groups. Graph measures including local efficiency, participation coefficient, diversity, and betweenness centrality have the greatest ability to differentiate and change between different age groups.

Areas including right putamen, amygdala, hippocampus, precuneus, anterior cingulate gyrus, superior occipital gyrus, right inferior temporal gyrus, cerebral cortex, temporal pole: middle temporal gyrus, middle temporal gyrus, and left inferior parietal are frequently repeated in important area. These areas have been identified in previous studies as age-varying areas [73, 74].

This research, however, is subject to some limitations including: first, due to variable health conditions associated with aging (e.g., brain amyloid status), a larger sample size is needed to draw more precise conclusions. Second, it should be noted that differences in spontaneous thoughts during fMRI acquisition may exist between different age groups. Third, the existence of intergenerational differences that may confound the results of neuroimaging research—especially in non-longitudinal studies.

For future studies, according to our results for local graph measures, it is also useful to evaluate graph measures at the voxel scale using large numbers of subjects. In addition, there are many methods for thresholding and determining the range of thresholds that can be used in future studies. Moreover, finding the optimal value of the thresholding can be investigated. Also, BOLD time series is a nonlinear signal in nature. Thus, the use of a nonlinear measure of connectivity can lead to more accurate results. Also, there are several key areas that warrant additional exploration. Firstly, we emphasize the importance of this study in informing the clinical trials design, particularly in terms of grouping participants based on resting state functional connectivity (RSFC). Additionally, future research should focus on the development of closed-loop interventions aimed at regulating RSFC, the neurophysiological prognosis of aging-related cognitive decline, and the association between fMRI-based metrics and EEG-based metrics for the ease of testing and data acquisition.

Conclusion

We employed an exploratory functional connectivity measure on the resting state fMRI data comprising three age groups to construct the corresponding brain network. The graph measures were extracted from the binary adjacency matrices. The Kruskal-Wallis test and the Fisher score were then used for selecting the best subset of features. The results showed that global efficiency and transitivity were significantly different between age groups in most of the thresholds. We also identified a subset of brain areas that showed significant differences between the three groups in most local network properties. In accordance with our findings, it seems that regions like amygdala, putamen, hippocampus, precuneus, inferior temporal gyrus, anterior cingulate gyrus, and middle temporal gyrus are the brain regions involved in age-related brain changes. Graph measures were also used for classification, employing different classification methods. The best classification accuracy was 82.2% using decision tree classifier and feature selection with Fisher score.

Funding Data were provided by the Human Connectome Project, WU-Minn Consortium (Principal Investigators: David Van Essen and Kamil Ugurbil; 1U54MH091657) funded by the 16 NIH Institutes and Centers that support the NIH Blueprint for Neuroscience Research; and by the McDonnell Center for Systems Neuroscience at Washington University.

Data Availability All the data used are from public databases and described and referenced properly in the manuscript.

Declarations

Competing interests The authors declare no competing interests.

References

1. Krampe RT. Aging, expertise and fine motor movement. Neurosci Biobehav Rev. 2002;26(7):769–76.
2. Grady C. The cognitive neuroscience of ageing. Nat Rev Neurosci. 2012;13(7):491–505.
3. Franke K, Ziegler G, Klöppel S, Gaser C, Initiative ADN. Estimating the age of healthy subjects from T1-weighted MRI scans using kernel methods: exploring the influence of various parameters. Neuroimage. 2010;50(3):883–92.
4. Varangis E, Habeck CG, Razlighi QR, Stern Y. The effect of aging on resting state connectivity of predefined networks in the brain. Front Aging Neurosci. 2019;11:234.
5. Roceanu A, Onu M, Badea L, Bajenaru O. Imaging brain networks—short presentation of new techniques. Rom J Neurol. 2013;12(4):180.
6. Finotelli P, et al. Exploring resting-state functional connectivity invariants across the lifespan in healthy people by means of a recently proposed graph theoretical model. PLoS One. 2018;13(11):e0206567.
7. Calhoun VD, Miller R, Pearlson G, Adalı T. The chronnectome: time-varying connectivity networks as the next frontier in fMRI data discovery. Neuron. 2014;84(2):262–74.
8. Tafreshi TF, Daliri MR, Ghodousi M. Functional and effective connectivity based features of EEG signals for object recognition. Cogn Neurodyn. 2019;13(6):555–66.
9. Cao M, et al. Topological organization of the human brain functional connectome across the lifespan. Dev Cogn Neurosci. 2014;7:76–93.
10. Friston KJ. Functional and effective connectivity in neuroimaging: a synthesis. Hum Brain Mapp. 1994;2(1–2):56–78.
11. Wang L, Su L, Shen H, Hu D. Decoding lifespan changes of the human brain using resting-state functional connectivity MRI. PLoS ONE. 2012;7(8):e44530.
12. Fair DA, et al. Functional brain networks develop from a 'local to distributed' organization. PLoS Comput Biol. 2009;5(5):e1000381.
13. Qiu A, Lee A, Tan M, Chung MK. Manifold learning on brain functional networks in aging. Med Image Anal. 2015;20(1):52–60.
14. Cai B, et al. Refined measure of functional connectomes for improved identifiability and prediction. Hum Brain Mapp. 2019;40(16):4843–58.
15. Cui Z, et al. Individual variation in functional topography of association networks in youth. Neuron. 2020;106(2):340–53.
16. Finn E, Shen X, Scheinost D, Rosenberg MD, Huang J, Chun MM, Papademetris X, Constable RT. Functional connectome fingerprinting: identifying individuals using patterns of brain connectivity. Nat Neurosci. 2015;18:1664–71.
17. Xiao L, et al. Distance correlation-based brain functional connectivity estimation and non-convex multi-task learning for developmental fMRI studies. IEEE Trans Biomed Eng. 2022;69(10):3039–50.
18. Rubinov M. Rubinov and sporns-2010—complex network measures of brain connectivity. Neuroimage. 2010;52:1059–69.
19. Song J, et al. Age-related reorganizational changes in modularity and functional connectivity of human brain networks. Brain Connect. 2014;4(9):662–76.
20. Sporns O. Graph theory methods: applications in brain networks. Dialogues Clin Neurosci. 2018;20(2):111–21.
21. Varangis E, Habeck CG, Stern Y. Task-based functional connectivity in aging: how task and connectivity methodology affect discovery of age effects. Brain Behav. 2021;11(1):e01954.
22. Javaid H, Kumarnsit E, Chatpun S. Age-related alterations in EEG network connectivity in healthy aging. Brain Sci. 2022;12(2):218.
23. Van Essen DC, Smith SM, Barch DM, Behrens TE, Yacoub E, Ugurbil K, Wu-Minn HCP Consortium et al. The WU-Minn human connectome project: an overview. Neuroimage. 2013;80:62–79.
24. Van Essen DC, Smith SM, Barch DM, Behrens TE, Yacoub E, Ugurbil K, Consortium W-MH, et al. Neuroimage. 2013;80:62.
25. Jenkinson M, Bannister P, Brady M, Smith S. Improved optimization for the robust and accurate linear registration and motion correction of brain images. Neuroimage. 2002;17(2):825–41.
26. Tzourio-Mazoyer N, et al. Automated anatomical labeling of activations in SPM using a macroscopic anatomical parcellation of the MNI MRI single-subject brain. Neuroimage. 2002;15(1):273–89.
27. Lee Rodgers J, Nicewander WA. Thirteen ways to look at the correlation coefficient. Am Stat. 1988;42(1):59–66.
28. Gamboa OL, et al. Working memory performance of early MS patients correlates inversely with modularity increases in resting state functional connectivity networks. Neuroimage. 2014;94:385–95.
29. Ashtiani SNM, et al. Altered topological properties of brain networks in the early MS patients revealed by cognitive task-related fMRI and graph theory. Biomed Signal Process Control. 2018;40:385–95.
30. Borgatti SP, Everett MG. A graph-theoretic perspective on centrality. Soc Networks. 2006;28(4):466–84.

31. Tononi G, Edelman GM, Sporns O. Complexity and coherency: integrating information in the brain. Trends Cogn Sci. 1998;2(12):474–84.
32. Newman MEJ. Modularity and community structure in networks. Proc Natl Acad Sci. 2006;103(23):8577–82.
33. Chiang S, Haneef Z. Graph theory findings in the pathophysiology of temporal lobe epilepsy. Clin Neurophysiol. 2014;125(7):1295–305.
34. Latora V, Marchiori M. Efficient behavior of small-world networks. Phys Rev Lett. 2001;87(19):198701.
35. Latora V, Marchiori M. Economic small-world behavior in weighted networks. Eur Phys J B-Condensed Matter Complex Syst. 2003;32(2):249–63.
36. Mari SI, Lee YH, Memon MS, Park YS, Kim M. Adaptivity of complex network topologies for designing resilient supply chain networks. Int J Ind Eng. 2015;22(1).
37. Rubinov M, Sporns O. Complex network measures of brain connectivity: uses and interpretations. Neuroimage. 2010;52(3):1059–69.
38. Humphries MD, Gurney K. Network 'small-world-ness': a quantitative method for determining canonical network equivalence. PLoS One. 2008;3(4):e0002051.
39. Zhang Z, et al. Altered functional–structural coupling of large-scale brain networks in idiopathic generalized epilepsy. Brain. 2011;134(10):2912–28.
40. Onias H, et al. Brain complex network analysis by means of resting state fMRI and graph analysis: will it be helpful in clinical epilepsy? Epilepsy Behav. 2014;38:71–80.
41. Hagmann P, et al. Mapping the structural core of human cerebral cortex. PLoS Biol. 2008;6(7):e159.
42. Lohmann G, et al. Eigenvector centrality mapping for analyzing connectivity patterns in fMRI data of the human brain. PLoS One. 2010;5(4):e10232.
43. Bullmore ET, Bassett DS. Brain graphs: graphical models of the human brain connectome. Annu Rev Clin Psychol. 2011;7:113–40.
44. Kruschwitz JD, List D, Waller L, Rubinov M, Walter H. GraphVar: a user-friendly toolbox for comprehensive graph analyses of functional brain connectivity. J Neurosci Methods. 2015;245:107–15.
45. McKight PE, Najab J. Kruskal-Wallis test. Corsini Encycl Psychol. 2010;1–1.
46. Kruskal WH, Wallis WA. Use of ranks in one-criterion variance analysis. J Am Stat Assoc. 1952;47(260):583–621.
47. Cherrington M, Thabtah F, Lu J, Xu Q. Feature selection: filter methods performance challenges. In Int Conf Comput Inf Sci (ICCIS). 2019;2019:1–4.
48. Azarmi F, Ashtiani SNM, Shalbaf A, Behnam H, Daliri MR. Granger causality analysis in combination with directed network measures for classification of MS patients and healthy controls using task-related fMRI. Comput Biol Med. 2019;115:103495.
49. Zhao Z, Morstatter F, Sharma S, Alelyani S, Anand A, Liu H. Advancing feature selection research. ASU feature selection repository. Repos. 2010;1–28.
50. Spolaôr N, Cherman EA, Monard MC, Lee HD. ReliefF for multi-label feature selection. In Braz Conf Intell Syst. 2013;2013:6–11.
51. Peng H, Long F, Ding C. Feature selection based on mutual information criteria of max-dependency, max-relevance, and min-redundancy. IEEE Trans Pattern Anal Mach Intell. 2005;27(8):1226–38.
52. Cortes C, Vapnik V. Support-vector networks. Mach Learn. 1995;20(3):273–97.
53. Abe S. Support vector machines for pattern classification. London: Springer, 2005;(2).
54. Song Y-Y, Ying LU. Decision tree methods: applications for classification and prediction. Shanghai Arch psychiatry. 2015;27(2):130.
55. Cunningham P, Delany SJ. K-nearest neighbour classifiers-a tutorial. ACM Comput Surv. 2021;54(6):1–25.
56. Refaeilzadeh P, Tang L, Liu H. Cross-validation. Encycl database Syst. 2009;5:532–8.
57. Geerligs L, Renken RJ, Saliasi E, Maurits NM, Lorist MM. A brain-wide study of age-related changes in functional connectivity. Cereb cortex. 2015;25(7):1987–99.
58. Bullmore E, Sporns O. The economy of brain network organization. Nat Rev Neurosci. 2012;13(5):336–49.
59. Foo H et al. Age-and sex-related topological organization of human brain functional networks and their relationship to cognition. Front Aging Neurosci. 2021;(13):758–97.
60. Blondel VD, Guillaume J-L, Lambiotte R, Lefebvre E. Fast unfolding of communities in large networks. J Stat Mech theory Exp. 2008;2008(10):P10008.
61. Ajilore O, Lamar M, Kumar A. Association of brain network efficiency with aging, depression, and cognition. Am J Geriatr Psychiatry. 2014;22(2):102–10.
62. Geerligs L, Renken RJ, Saliasi E, Maurits NM, Lorist MM. A brain-wide study of age-related changes in functional connectivity. 2015;(July):1987–1999. https://doi.org/10.1093/cercor/bhu012
63. Elsheikh S, Chimusa ER, Mulder N, Crimi A. Relating connectivity changes in brain networks to genetic information in Alzheimer patients. In 2018 IEEE 15th Int Symp Biomed Imaging (ISBI 2018). 2018;1390–1393.
64. Mårtensson G, et al. Stability of graph theoretical measures in structural brain networks in Alzheimer's disease. Sci Rep. 2018;8(1):1–15.
65. Hagmann P, Cammoun L, Gigandet X, Meuli R, Honey CJ, Wedeen VJ. Mapping the structural core of human cerebral cortex. 2008;6 (7). https://doi.org/10.1371/journal.pbio.0060159
66. Talati A, Hirsch J. Functional specialization within the medial frontal gyrus for perceptual go/no-go decisions based on 'what','when', and 'where' related information: an fMRI study. J Cogn Neurosci. 2005;17(7):981–93.
67. Amunts K, et al. Cytoarchitectonic mapping of the human amygdala, hippocampal region and entorhinal cortex: intersubject variability and probability maps. Anat Embryol (Berl). 2005;210(5):343–52.
68. Jacques PS, Dolcos F, Cabeza R. Effects of aging on functional connectivity of the amygdala during negative evaluation: a network analysis of fMRI data. Neurobiol Aging. 2010;31(2):315–27.
69. Xu X, Kuang Q, Zhang Y, Wang H, Wen Z, Li M. Age-related changes in functional connectivity between young adulthood and late adulthood. Anal Methods. 2015;7(10):4111–22.
70. Khazaee A, Ebrahimzadeh A, Babajani-Feremi A. Application of advanced machine learning methods on resting-state fMRI network for identification of mild cognitive

impairment and Alzheimer's disease. Brain Imaging Behav. 2016;10(3):799–817.
71. Onoda K, Ishihara M, Yamaguchi S. Decreased functional connectivity by aging is associated with cognitive decline. J Cogn Neurosci. 2012;24(11):2186–98.
72. Yamaguchi S, Levy RM, Braga R. Decreased functional connectivity by aging is associated with cognitive decline. J Cogn Neurosci. 2012;24(11):2186-98.
73. Li L, Cazzell M, Babawale OM, Liu H. Automated voxel classification used with atlas-guided diffuse optical tomography for assessment of functional brain networks in young and older adults. Neurophotonics. 2016;3(4):45002.
74. Ai J, Liu T, Wang K, Yan T, Zhang, Huang T. Alterations of brain functional networks in older adults: a resting-state fMRI study using graph theory. In 2020 13th Int Congr Image Signal Process, BioMed Eng Informa (CISP-BMEI). 2020;372–377.